J Nanopart Res (2016) 18: 383
DOI 10.1007/s11051-016-3690-9

RESEARCH PAPER

The magnetization reversal in $CoFe_2O_4/CoFe_2$ granular systems

J. Jin · X. Sun · M. Wang · Z.L. Ding · Y.Q. Ma

Received: 29 June 2016 / Accepted: 29 November 2016 / Published online: 17 December 2016

Abstract The temperature-dependent field cooling (FC) and zero-field cooling (ZFC) magnetizations, i.e., M_{FC} and M_{ZFC}, measured under different magnetic fields from 500 Oe to 20 kOe have been investigated on two exchange–spring $CoFe_2O_4/CoFe_2$ composites with different relative content of $CoFe_2$. Two samples exhibit different magnetization reversal behaviors. With decreasing temperature, a progressive freezing of the moments in two composites occurs at a field-dependent irreversible temperature T_{irr}. For the sample with less $CoFe_2$, the curves of $-d(M_{FC} - M_{ZFC})/dT$ versus temperature T exhibit a broad peak at an intermediate temperature T_2 below T_{irr}, and the moments are suggested not to fully freeze till the lowest measuring temperature 10 K. However, for the $-d(M_{FC} - M_{ZFC})/dT$ curves of the sample with more $CoFe_2$, besides a broad peat at an intermediate temperature T_2, a rapid rise around the low temperature T_1~15 K is observed, below which the moments are suggested to fully freeze. Increase of magnetic field from 2 kOe leads to the shift of T_2 and T_{irr} towards a lower temperature, and the shift of T_2 is attributable to the moment reversal of $CoFe_2O_4$.

Keywords $CoFe_2O_4/CoFe_2$ · Reentrant spin-glass · Exchange–spring · Dipolar interaction · Magnetic properties · Nanocomposites

Research highlights
1. The magnetization reversal behavior of $CoFe_2O_4/CoFe_2$ was investigated.
2. The content of $CoFe_2$ affects the magnetization reversal behaviors.
3. The reentrant spin-glass state was observed in the sample with more $CoFe_2$.

J. Jin · X. Sun · M. Wang · Z. Ding · Y. Ma
Anhui Key Laboratory of Information Materials and Devices, School of Physics and Materials Science, Anhui University, Hefei 230601, People's Republic of China

Y. Ma (✉)
Engineering Technology Research Center of Magnetic Materials, Anhui Province, People's Republic of China
e-mail: yqma@ahu.edu.cn

Introduction

Hard $CoFe_2O_4$/soft CoFe composite has been extensively investigated recently (Quesada et al. 2014; Zan et al. 2013a, b; Ou-Yang et al. 2015) in order to obtain high coercivity (H_c), saturation magnetization (M_s), and the remanence (M_r) to saturation magnetization ratio (M_r/M_s) through the exchange–coupling between hard ferrimagnetic $CoFe_2O_4$ with high H_c and soft ferromagnetic CoFe with high M_s (Qin et al. 2009; Zhang et al. 2011; Zehani et al. 2014; Aguirre Mdel et al. 2015; Xu et al. 2015c; Cernea et al. 2016; Ramis Mustafa et al. 2014). Unfortunately, most previous reports revealed that M_r/M_s was smaller than 0.5 (Quesada et al. 2014; Soares et al. 2014; Soares et al. 2011). This may result from the complex interactions, besides the exchange–coupling interaction, as discussed below, which affects the magnetization reversal and consequently influences on the macroscopic magnetic properties. This issue has not been investigated in detail before for the $CoFe_2O_4$/CoFe composite as far as we know.

If the exchange–coupling occurs between hard and soft phases, the magnetization of the soft and hard phases could show an equivalent reversal behavior in the whole temperature region, and thus, the magnetization changes with the external magnetic field smoothly, exhibiting the characteristic of single-phase hard magnet (López-Ortega et al. 2015; Xia et al. 2015; Hamid and Ahmad Khalid 2011). However, some reports observed the exchange–uncoupled (Quesada et al. 2014) or the exchange–spring effect (Zhang et al. 2013) in $CoFe_2O_4$/$CoFe_2$ composites, and the hysteresis loops exhibited a jump in the low field region as a result of the broad distribution of reversal fields of hard and soft species (Quesada et al. 2014). Besides the exchange interaction (exchange–coupling and exchange–spring) occurring at the interface between $CoFe_2O_4$ and $CoFe_2$, the dipolar interaction between $CoFe_2O_4$/$CoFe_2$ particles can lead to the formation of spin-glass state in which the particle moment orients randomly, and the dipolar interaction is suggested to suppress the M_r/M_s value (Xu et al. 2015a; Geng et al. 2016a, b; Geng et al. 2015; Wang et al. 2012). The strength of dipolar interaction can be estimated by the dipolar field H_{dip}, defined as $H_{dip} = 2\ \mu/d^3$, where μ is the particle moment ($\mu = M_s \times V_m$; M_s is the saturation magnetization and V_m is magnetic grain volume) and d is the distance between particles (center to center). Therefore, the cooperative effects of exchange–spring, exchange–coupling, and dipolar interaction as well as the anisotropy modify the energy barrier distribution, which influence on the magnetization reversal and consequently on the magnetic properties (Kooti and Naghdi Sedeh 2013).

The energy barrier distribution, f (T), can be investigated by the measurements of field cooling (FC) and zero-field cooling (ZFC) magnetizations, i.e., M_{FC} and M_{ZFC}, because f (T) can be calculated by (Pianciola Betiana et al. 2015; Bianco et al. 2002) $f(T) - d(M_{FC} - M_{ZFC})/dT$. The energy barrier distribution affects the magnetic properties and magnetic ordering state, as observed in Co_3O_4 (Mousavand et al. 2009; Benitez et al. 2008), $CoFe_2O_4$ (Pianciola Betiana et al. 2015), $NiFe_2O_4$ nanoparticles diluted by SiO_2 (Nadeem et al. 2014), nanostructure of exchange–coupled Fe core with Fe oxide shell (Bianco et al. 2002), Ni/NiO core–shell nanoparticles (Ji et al. 2015), and ε-$Fe_{3-x}Ni_xN$ (Gajbhiye and Bhattacharyya 2008). In the present work, the M_{FC} and M_{ZFC} measured at different magnetic fields from 500 Oe to 20 kOe were investigated on two exchange–spring $CoFe_2O_4$/$CoFe_2$ composites with different relative content of $CoFe_2$, throwing light on some aspects of magnetization reversal behavior that to our knowledge were not addressed in previous investigations on $CoFe_2O_4$/$CoFe_2$ systems.

Experimental procedure

The synthesis of $CoFe_2O_4$ (hard)/$CoFe_2$ (soft) nanocomposites was carried out by two steps: monodispersed $CoFe_2O_4$ nanoparticles were first synthesized by the thermal decomposition of $Fe(acac)_3$ and $Co(acac)_2$ in organic solvent of benzyl ether, oleic acid, and oleylamine as described elsewhere (Xu et al. 2015a); then, the $CoFe_2O_4$ nanoparticles were reduced in the H_2 ambient at 300 °C (500 sccm, 96%N_2 + 4%H_2) for 4 and 8 h to obtain the final samples, which are hereafter referred to as the samples S4H and S8H, respectively.

The crystal structure of the products was determined by X-ray diffraction (XRD) using an X-ray diffractometer (XRD; DX-2000 SSC, Dandong Fangyuan Instrument Company, DanDong, Liaoning, China) with Cu Kα irradiation (λ = 1.5406 Å) in the scanning range 20–80° with a step size of 0.02°. The (high resolution) transmission electron microscopy ((HR)TEM; JEOL JEM-2100, Tokyo, Japan) was used to observe the particle size, morphology, and lattice fringes. The distribution trends of O, Fe, and Co elements were detected by EDS elemental mapping analysis. Magnetic measurements were carried out using a superconducting quantum interference device PPMS system (SQUID, PPMS EC-II, Quantum Design Inc., San Diego, California, USA).

Results and discussion

Crystal structure and morphology

As-prepared $CoFe_2O_4$ (Fig. 1b) exhibited the single-phase cubic spinel structure, compared with the powder diffraction file (PDF) of $CoFe_2O_4$ (No: 22–1086) in Fig. 1a. After $CoFe_2O_4$ was reduced in H_2 for 4 h, the obtained sample, i.e., S4H (Fig. 1c), appeared in the reflection of $CoFe_2$ alloy according to the PDF card of $CoFe_2$ (No: 65–4131) in Fig. 1e, due to the reducing reaction: $CoFe_2O_4 + 4H_2 \rightarrow CoFe_2 + 4H_2O$ (Soares et al. 2011). For the S8H sample, as shown in Fig. 1d,

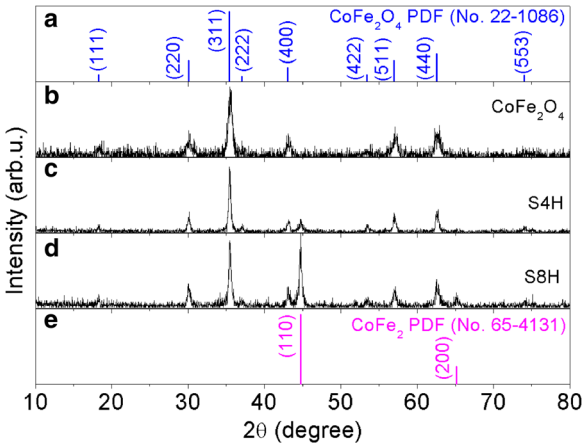

Fig. 1 X-ray diffraction patterns of as-prepared $CoFe_2O_4$ (**b**), S4H (**c**), and S8H (**d**); the standard PDF cards of $CoFe_2O_4$ (**a**) and $CoFe_2$ (**e**)

the diffraction intensity of $CoFe_2$ increases due to the longer duration in the H_2/N_2 atmosphere.

As shown in Fig. 2a, the as-prepared $CoFe_2O_4$ comprises the well-dispersed nanoparticles. The particle size ranges from 26 to 34 nm, as illustrated in the size histogram in Fig. 2c. The average particle size, defined as the size corresponding to the peak of the Gaussian fitting curve (solid line), is ~30.4 nm. The (HR)TEM image in Fig. 2b shows the clear fringes with the interfringe distance 0.48 nm, corresponding to the (111) crystal plane of $CoFe_2O_4$ (Sun et al. 2015). After $CoFe_2O_4$ is reduced for 8 h, the particles in the S8H sample aggregate to some extent as shown in Fig. 2g. The (HR)TEM can only detect the fringes from $CoFe_2$, as shown in Fig. 2h, indicating that the reduction of $CoFe_2O_4$ occurs first at the surface of particle, i.e., $CoFe_2$ exists at the outer layer while $CoFe_2O_4$ exists in the inner of particle. As seen in the EDS spectra of $CoFe_2O_4$ and S8H in Fig. 2i, the intensity of O in S8H is obviously lower than that in $CoFe_2O_4$ due to the loss of O after reduction of $CoFe_2O_4$. From the elemental mapping for O, Fe, and Co, it can be observed that the distribution of O element in $CoFe_2O_4$ is more uniform than in S8H, as shown in Fig. 2d, j. Compared with the elemental mapping of Fe and Co in $CoFe_2O_4$ (Fig. 2e, f),

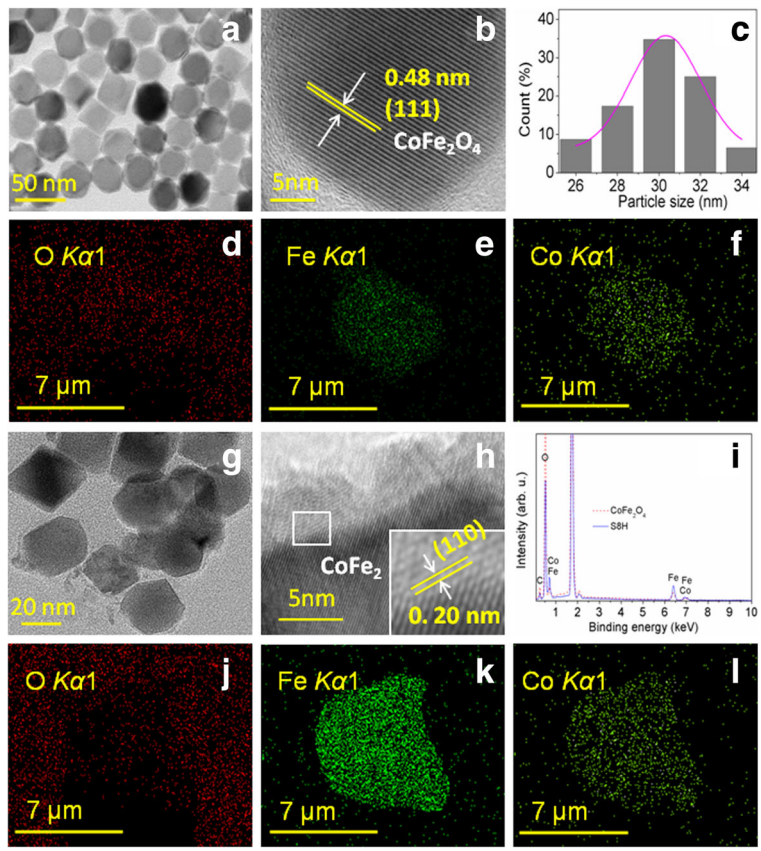

Fig. 2 The TEM image (**a**), HRTEM image (**b**), size histogram with Gaussian-fitting curve (*solid line*) (**c**), and EDS elemental mapping for O (**d**), Fe (**e**), and Co (**f**) of the as-prepared $CoFe_2O_4$; the TEM image (**g**) and HRTEM image (**h**) of the S8H sample, an energy dispersive spectroscopy (EDS) of $CoFe_2O_4$ and S8H (**i**), and elemental mapping for O (**j**), Fe (**k**), and Co (**l**) of S8H. The *inset* in **h** shows the magnified detail of *square-marked area*

the S8H sample (Fig. 2k, l) exhibits a clearer contrast, which means a higher concentration of Fe and Co in the S8H sample.

The magnetic field (H)-dependent magnetization (M) curves, i.e., $M(H)$ loops (−70 kOe < H < + 70 kOe) recorded at 10 and 300 K for the S4H and S8H samples, were shown in Fig. 3. A jump appears in $M(H)$ loop of 10 K around $H = 0$ for the S4H sample, which can be attributed to the broad distribution of reversal fields of hard $CoFe_2O_4$ and soft $CoFe_2$ species (Quesada et al. 2014). The jump is enhanced for S8H because of the more soft $CoFe_2$ component (Sun et al. 2015). Furthermore, the jump also signifies that no exchange–coupling but exchange–spring effect occurs at the interface between $CoFe_2O_4$ and $CoFe_2$ because in the exchange–coupled $CoFe_2O_4$ and $CoFe_2$ system, their magnetizations could have an equivalent reversal behavior in the whole temperature region, leading to a smooth hysteresis loop which is characteristic of a single-phase hard magnet (López-Ortega et al. 2015). The similar exchange–spring effect was reported before for $CoFe_2O_4/CoFe_2$ (Zhang et al. 2013) and Fe/Sm-Co (Liu et al. 2011). With increasing temperature, the anisotropy field of $CoFe_2O_4$ strongly decreases with increasing temperature, and consequently, the average reversal fields of hard and soft phases may be similar, resulting in the single-phase behavior of loops of 300 K, i.e., the smooth loops. The M_s values are 96 emu/g (10 K) and 92 emu/g (300 K) for S4H and 118 emu/g (10 K) and 115 emu/g (300 K) for S8H. S8H has the larger M_s value than S4H because of more $CoFe_2$ existing in S8H. The H_c values are 11.8 kOe (10 K) and 1.7 kOe (300 K) for S4H and 2.5 kOe (10 K) and 1.2 kOe (300 K) for S8H. H_c of S8H is smaller than that for S4H. For the soft and hard composite system, the effective anisotropy constant K is expressed by $K = f_sK_s + f_hK_h$, where f_s and f_h are the volume fraction and K_s and K_h are the anisotropy constant of soft and hard phases with $K_s \ll K_h$, respectively (Zan et al. 2013a; Geng et al. 2015); S8H has more $CoFe_2$, therefore it has smaller K and hence smaller H_c due to $H_c \propto K$.

Figure 4 shows the field derivative dM/dH of the virgin curves at 10 K for S4H and S8H samples, and the magnetic field at the peak of dM/dH curve is the irreversible magnetization reversal field (H_{irr}). Two peaks locate at 3.4 and 20 kOe for the S4H sample, and at 2.4 and 16 kOe for the S8H sample, the peaks at low and high field, respectively, corresponding to the irreversible magnetization reversal of $CoFe_2$ and $CoFe_2O_4$. $CoFe_2$ is a typical soft magnet with small anisotropy, so it has small H_{irr}. More $CoFe_2O_4$ in an individual particle for the S4H sample exerts the pinning effect on the moment of $CoFe_2$, leading to the H_{irr}

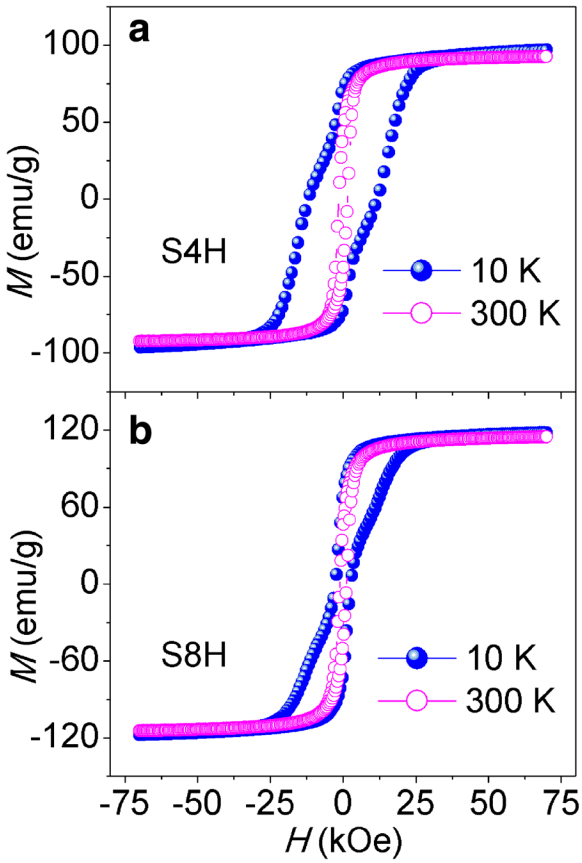

Fig. 3 $M(H)$ loops for the S4H (**a**) and S8H (**b**) samples measured at 10 and 300 K

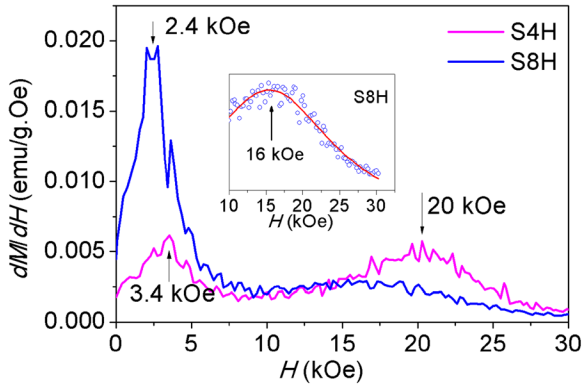

Fig. 4 The field derivative dM/dH of the virgin curves for S4H and S8H samples at 10 K. The *inset* shows the local dM/dH data (*empty circles*) around 16 kOe of the S8H sample with the curve of Lorentz fit (*solid line*) in order to find the peak position

increase of $CoFe_2$, while more $CoFe_2$ in S8H polarizes the moments of $CoFe_2O_4$, resulting in the H_{irr} decrease of $CoFe_2O_4$ (Bianco et al. 2002). The appearance of two peaks is also indicative of two-phase feature of magnetization reversal, i.e., exchange–spring rather than exchange–coupling between $CoFe_2O_4$ and $CoFe_2$.

Figure 5 shows the zero-field cooling (ZFC) and field cooling (FC) magnetization (M) curves of the sample S4H from 10 to 390 K, recorded at different applied magnetic fields H from 500 Oe to 20 kOe. The FC and ZFC curves for the low fields of H = 500 Oe and 1 kOe do not overlap up to 390 K, and both the ZFC and FC curves decrease with lowering temperature; these behaviors signify the existence of the super-spin-glass (SSG) state as a result of the strong dipolar interaction (Xu et al. 2015a, b, c; Petracic et al. 2006). In the case of H ≥ 2 kOe, the FC and ZFC curves overlap at the irreversibility temperature (T_{irr}), defined as the temperature where $M_{FC} - M_{ZFC}$ is about 5% (Bianco et al. 2002). Below T_{irr}, the FC and ZFC curves bifurcate. T_{irr} decreases with increasing H, and the variation of T_{irr} with H is plotted in Fig. 11a. On increasing H from 2 to 20 kOe, T_{irr} reduces, but the magnetic irreversibility persists at low temperature even under the largest field of H = 20 kOe. Below T_{irr}, the particle moments are blocking or freezing while they exhibit a ferromagnetic-like trend above T_{irr}. With increasing H, the shape of the ZFC curve depends strongly on the field: M_{ZFC} decreases monotonically with the temperature for H < 3 kOe while it first exhibits a peak and then decreases for H > 3 kOe. M_{ZFC} decreases in the low-temperature region because the unfrozen disordered moments tend to the frozen SSG state at low temperature, in which the moments are pointing randomly into all directions.

As shown in Fig. 6, the FC and ZFC curves of the S8H sample exhibit the following features:

1) For all the applied fields, first, the M_{FC} monotonically increases till 50 K, where a peak appears, and

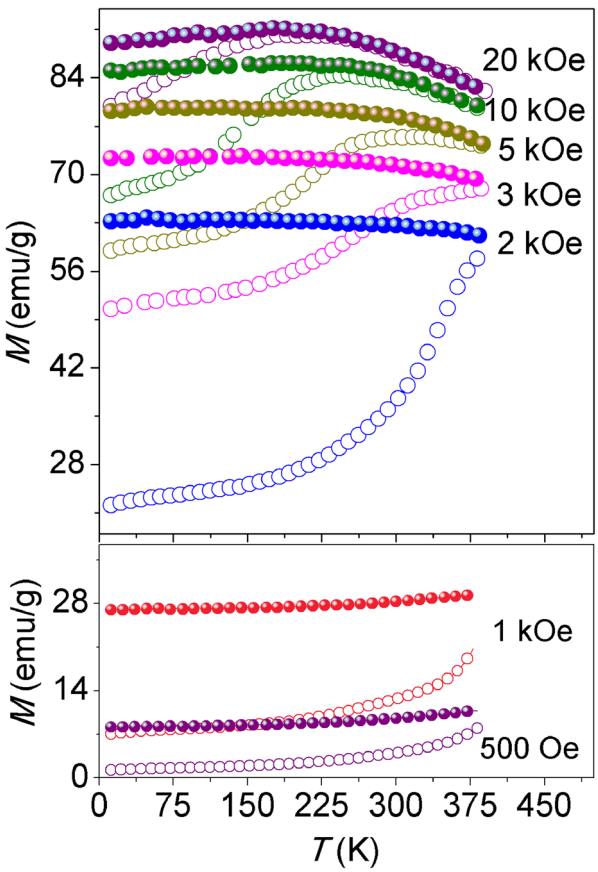

Fig. 5 ZFC (*empty circles*) and FC (*solid circles*) magnetization (M) curves of the S4H sample for different applied magnetic fields

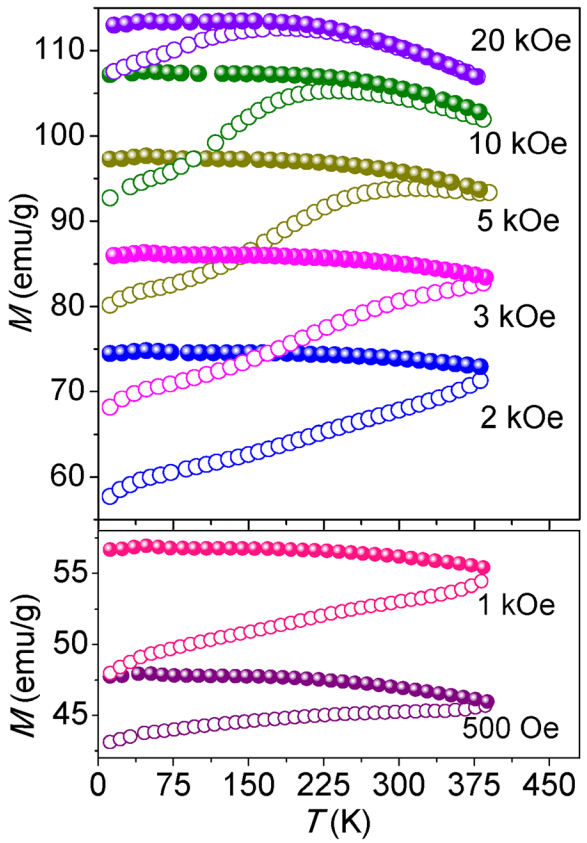

Fig. 6 ZFC (*empty circles*) and FC (*solid circles*) magnetization (M) curves of the S8H sample for different applied magnetic fields

then decreases as the temperature is reduced. In order to clearly show the peak position, M_{FC} in Fig. 6 was divided by the maximum of M_{FC}, i.e., normalized M_{FC}, and Fig. 7 representatively shows the normalized M_{FC} curves for H = 2, 5, and 20 kOe. The peak position does not change with H. Such peak is not observed in the S4H sample; so, it can be suggested that the peak relates to more $CoFe_2$ in S8H. The similar peak has been observed in $CoFe_2$ alloy with minimal $CoFe_2O_4$ and Fe_2O_3 (Geng et al. 2016a, b), further confirming that more $CoFe_2$ is responsible for the peak around 50 K. A local maximum or peak in the M_{FC} curve signifies the existence of the SSG state (Mathieu et al. 2013), which typically exhibit glass temperature around 50 K (Petracic et al. 2006). Imaginably, the collective effects of exchange–spring, occurring at the interface of $CoFe_2O_4$ and $CoFe_2$, and the dipolar interaction, occurring between $CoFe_2O_4$/$CoFe_2$ particles, together with the random anisotropy of $CoFe_2O_4$, result in the breakdown of long-range ferromagnetic order in $CoFe_2$ and the frustrated configurations of moments at low temperature, i.e., reentrant spin-glass. The orientation of moments is shown in Fig. 8. Therefore, the S8H sample passes from a paramagnetic, which occur at higher temperature beyond our measuring range, to a ferromagnetic and to a "reentrant" spin-glass phase as the temperature is reduced, as what occurs in ε-$Fe_{3-x}Ni_xN$ ($0.1 \le x \le 0.8$) (Gajbhiye and Bhattacharyya 2008).

2) T_{irr} of S8H, shown in Fig. 11b, is lower than that of S4H. The S8H sample has more soft $CoFe_2$ with smaller anisotropy than $CoFe_2O_4$; so, it has the smaller effective anisotropy K than S4H, leading to the decrease in T_{irr} which can be deduced from $KV = 25\ k_BT_{irr}$ (Verma and Pravarthana 2011), where V is the volume of the particle and k_B is the Boltzmann constant.

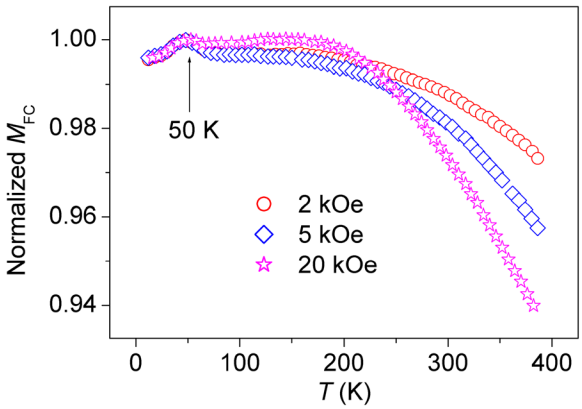

Fig. 7 Normalized M_{FC} by the maximum of M_{FC} with H = 2, 5, and 20 kOe

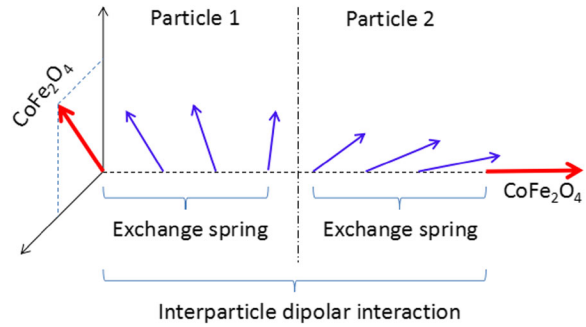

Fig. 8 Schematic plot for the moment orientation in the S8H sample. *Red arrow* denotes the moment of $CoFe_2O_4$ and *blue arrow* denotes the moment of $CoFe_2$

The temperature derivative of the difference between the FC and ZFC magnetization ($M_{FC} - M_{ZFC}$), i.e., $-d(M_{FC} - M_{ZFC})/dT$, has been calculated. The data of $-d(M_{FC} - M_{ZFC})/dT$ versus temperature T are shown in Fig. 9 for the S4H sample and fitted by a Lorentz function in order to read the peak temperature accurately. In the cases of H = 500 Oe and 1 kOe, $-d(M_{FC} - M_{ZFC})/dT$ does not exhibit the peak in the temperature region 10~390 K, while a broad peak appears at T_2 = 348 K when H increases to 2 kOe (Fig. 9a) and the peak shifts to lower temperature as H increases, as shown in Fig. 11a. This peak has also been observed in Fe/Fe oxide granular system (Bianco et al. 2002). In the Fe/Fe oxide system, $-d(M_{FC} - M_{ZFC})/dT$ exhibits two peaks which locate at low-temperature T_1 and at high-temperature T_2. The low-temperature region below T_1 corresponds to the completely frozen state. The region between T_1 and T_2 defines a regime consisting of frozen and relaxing oxide magnetic regions, which coexist with the quasistatic Fe component. However, the S4H sample does not exhibit the quasistatic T_1 peak, maybe indicating that the moments are not fully frozen until 10 K. Fig. 9 The temperature derivative of the difference between the FC and ZFC magnetization ($M_{FC} - M_{ZFC}$), i.e., the curves of $-d(M_{FC} - M_{ZFC})/dT$ versus temperature T, for the S4H sample. The solid line is the fitting curve according to the Lorentz function.

Furthermore, the broad and relaxing peak at T_2 indicates the existence of a very broad, field-dependent energy barrier distribution. This is supported by the irreversibility below T_{irr}, by the field-dependent $M_{FC} - M_{ZFC}$ at 10 K and

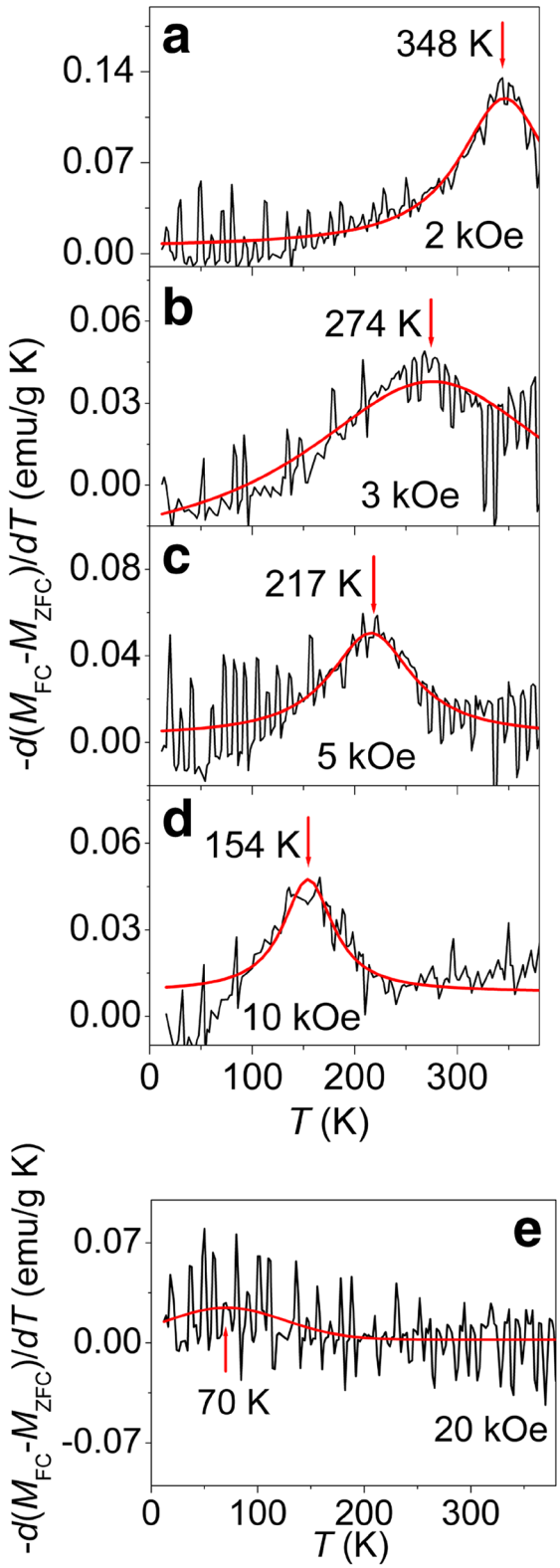

Fig. 9 The temperature derivative of the difference between the FC and ZFC magnetization ($M_{FC} - M_{ZFC}$), i.e., the curves of $-d(M_{FC} - M_{ZFC})/dT$ versus *temperature T*, for the S4H sample. The *solid line* is the fitting curve according to the Lorentz function

by the decrease of T_{irr} with increasing H above 2 kOe. T_{irr} signals the onset of a freezing process with decreasing temperature, i.e., the blocking associated to the highest anisotropy energy barrier (Bianco et al. 2002).

For the S8H sample, the $-d(M_{FC} - M_{ZFC})/dT$ curves do not appear at a peak for H = 500 Oe and 1 kOe (not shown here). The curves in Fig. 10 with H ≥ 2 kOe exhibit the following characteristics: (1) In the low-temperature region, M_{FC} rapidly rises with decreasing temperature till T_1~15 K, and the shape of curve is not sensitive to the magnetic field, exhibiting the quasistatic characteristic, as what occurred in Fe/Fe oxide (Bianco et al. 2002). The feature of curve around T_1~15 K is not observed in the S4H sample; so, it may be related to the reentrant spin-glass state in S8H with more $CoFe_2$, or in other words, $CoFe_2$ contributes to the quasistatic curve around T_1~15 K. In the Fe/Fe oxide, a quasistatic peak appears at T_1~20 K and a low-temperature region below T_1~20 K corresponds to the frozen and disordered magnetic state, characterized by a strong exchange–coupling between the structurally disordered, spin-glass-like oxide matrix, and the Fe nanocrystallites (Bianco et al. 2002). In the S8H sample, the rapid rise of $-d(M_{FC} - M_{ZFC})/dT$ in the low-temperature region is suggested to have the same origin as that in the Fe/Fe oxide, i.e., below T_1~15 K, there are fully frozen moments including disordered moments at the interface of the exchange–spring $CoFe_2O_4$ and $CoFe_2$ and those in reentrant spin-glass state. (2) On increasing the temperature above 15 K, the completely frozen state becomes progressively unfrozen. Between T_1 and T_{irr}, a broad peak appears at T_2 = 224 K for H = 2 kOe, which shifts to lower temperature as H increases, i.e., it is a relaxing peak. The dependence of T_1 and T_2 on H is shown in Fig. 11b. According to the field derivative dM/dH of the virgin curves for S4H and S8H samples at 10 K (see Fig. 4), it can be suggested that the moment reversal of $CoFe_2$ towards the magnetic field direction is almost completed at H = 3.4 kOe for S4H and H = 2.4 kOe for S8H. Therefore, it is reasonable to attribute the shift of T_2 peak occurring at higher field than 2 kOe to the moment reversal of $CoFe_2O_4$, which is determined by the cooperative effects of crystalline-anisotropy of $CoFe_2O_4$, exchange–spring effect between $CoFe_2O_4$ and $CoFe_2$ together with the inter-particle dipolar interaction. Furthermore, the increase in magnetic field favors

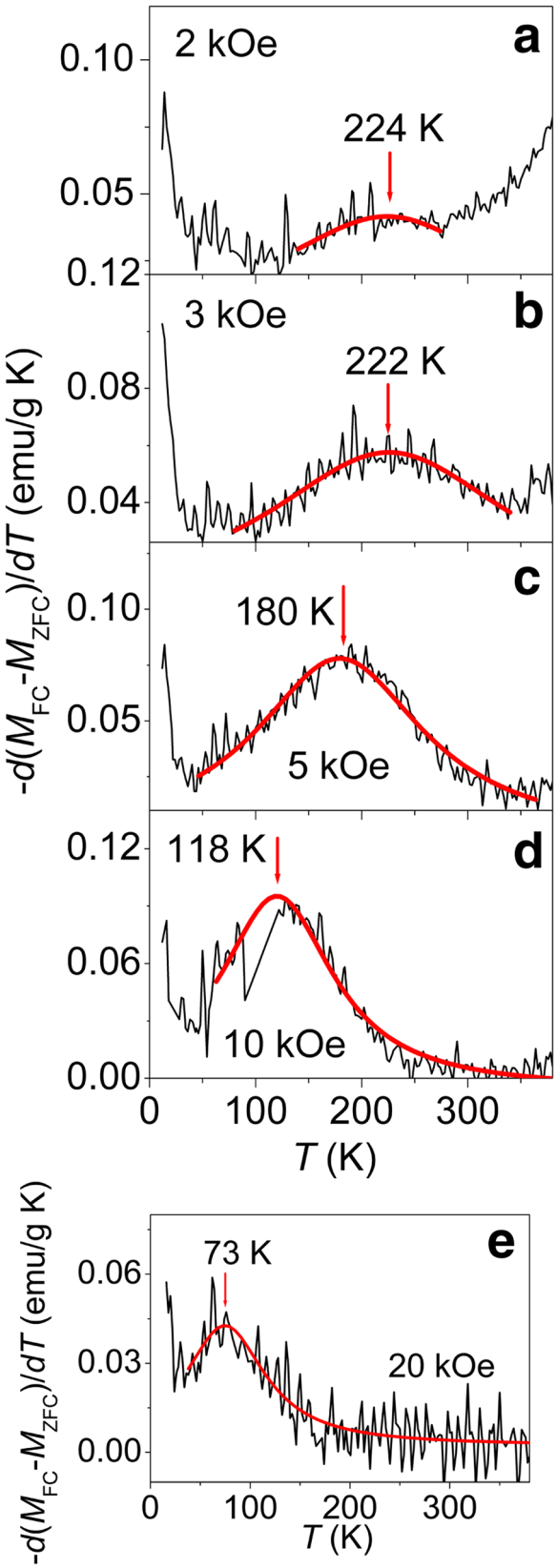

Fig. 10 The curves of $-d(M_{FC} - M_{ZFC})/dT$ versus temperature T for the S8H sample. The *solid line* is the fitting curve according to the Lorentz function

the formation of a ferromagnetic network throughout the sample, resulting in the shift of temper-ature for moment freezing or blocking towards a lower value, and consequently the decrease in T_2 and T_{irr} Fig. 10 The curves of $-d(M_{FC} - M_{ZFC})/dT$ versus temperature T for the S8H sample. The solid line is the fitting curve according to the Lorentz function.

Summarily, the intra- and inter-particle interaction and anisotropy determine the magnetization reversal in $CoFe_2O_4/CoFe_2$ granular systems, and consequently affect the magnetic properties, resulting in the different H_c, M_s, and M_r/M_s. These can be controlled by changing the content of $CoFe_2$ in $CoFe_2O_4/CoFe_2$ to obtain the desirable magnetic properties, which is meaningful for the practical applications such as the magnetic record medium and flexi-programmable logic devices [Li et al. 2015]. For example, the magnetic unit in magnetic record medium requires the suitable moment, anisotropy, and inter-particle interaction to stabilize the moment of the magnetic unit. As

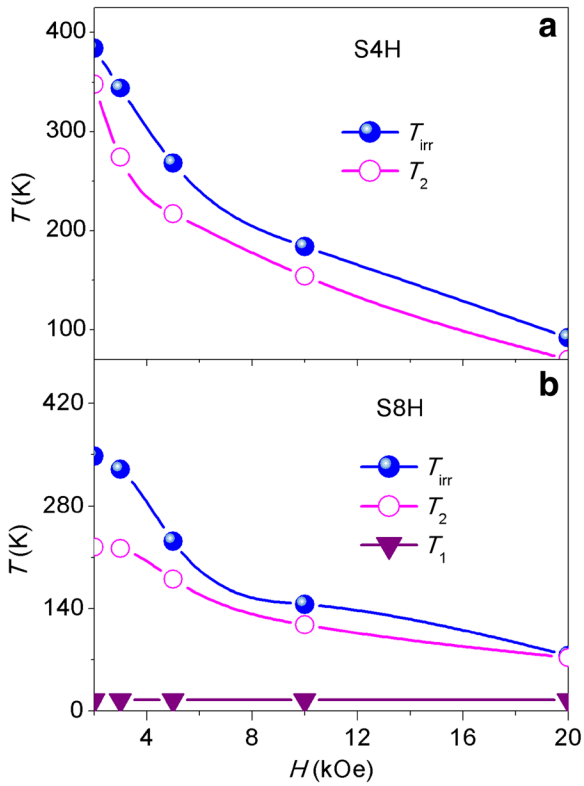

Fig. 11 Dependence of T_1, T_2, and T_{irr} on the applied magnetic field H for S4H (**a**) and S8H (**b**). The *inset* in **b** shows the T_2 of S4H and S8H versus H

is well-known, the distribution of hard and soft magnetic phases affects the magnetic properties of hard/soft composites. It deserves the further investigation to synthesize the nanostructures with the metal core/oxide shell, such as $CoFe_2$ (core)/$CoFe_2O_4$ (shell) and Fe (core)/Fe_2O_3 (shell). Furthermore, these nanostructures are expected to be promising materials for various bio-sensing applications because the oxide shell is biocompatible. Further investigations are in process.

Conclusions

The $CoFe_2O_4$/$CoFe_2$ composites were synthesized by the reduction of dispersive and uniform $CoFe_2O_4$ nanoparticles in H_2 ambient for 4 and 8 h in order to increase the relative content of $CoFe_2$, and the temperature-dependent magnetization was measured under different magnetic fields from 500 Oe to 20 kOe. The nature of the interplay between $CoFe_2O_4$ and $CoFe_2$ is the exchange–spring which can be observed in the hysteresis loops at 10 K. The magnetic properties of these two composites were determined by the anisotropy, intra-particle exchange–spring, and inter-particle dipolar interaction. The main results are as follows.

With decreasing temperature, a progressive freezing of the moments in two composites occurs at field-dependent irreversible temperature T_{irr}. The sample with more $CoFe_2$ has lower T_{irr} due to smaller anisotropy. In the case of the S4H sample, the moments are not fully frozen till the lowest measuring temperature. In the case of the S8H sample, it contains more $CoFe_2$; the long-range ferromagnetic ordering of $CoFe_2$ is broken down due to the cooperative effects of random anisotropy of $CoFe_2O_4$, the exchange–spring between $CoFe_2O_4$ and $CoFe_2$, and the inter-particle dipolar interaction, leading to the formation of the reentrant spin-glass state around 50 K. Below T_1~15 K, these disordered moments are fully frozen.

The increase in magnetic field from 2 kOe promotes the formation of a ferromagnetic network throughout the sample and suppresses the freezing or blocking of the moments, leading to the decrease of T_2 and T_{irr}. The shift of T_2 peak towards the lower temperature as H increases from 2 kOe can be attributed to the moment reversal of $CoFe_2O_4$, which is determined by the cooperative effects of crystalline-anisotropy of $CoFe_2O_4$, exchange–spring effect between $CoFe_2O_4$ and $CoFe_2$ together with the inter-particle dipolar interaction.

The results in the present work are meaningful for the practical applications such as the magnetic record medium and flexi-programmable logic devices.

Acknowledgments This work was supported by the National Natural Science Foundation of China (Grant Nos. 51471001, 11174004, and 11304001).

Compliance with ethical standards

Conflict of interest The authors declare that they have no conflict of interest.

References

Aguirre Mdel C, Farías E, Abraham J, Urreta SE (2015) $Co_{100-x}Fe_x$ magnetic thick films prepared by electrodeposition. J Alloy Compd 627:393–401

Bianco LD, Fiorani D, Testa AM, Bonetti E, Savini L, Signoretti S (2002) Magnetothermal behavior of a nanoscale Fe/Fe oxide granular system. Phys Rev B 66:174418

Benitez MJ, Petracic O, Salabas EL, Radu F, Tüysüz H, Schüth F, Zabel H (2008) Evidence for core-shell magnetic behavior in antiferromagnetic Co_3O_4 nanowires. Phys Rev Lett 101: 097206

Cernea M, Galizia P, Ciuchi I, Aldica G, Mihalache V, Diamandescu L, Galassi C (2016) $CoFe_2O_4$ magnetic ceramic derived from gel and densified by spark plasma sintering. J Alloys Compd 656:854–862

Gajbhiye NS, Bhattacharyya S (2008) Spin-glass-like ordering in ε-$Fe_{3-x}Ni_xN$ ($0.1 \le x \le 0.8$) nanoparticles. Mater Chem Phys 108:201–207

Geng BQ, Ding ZL, Ma YQ (2016a) Unraveling the correlation between the remanence ratio and the dipolar field in magnetic nanoparticles by tuning concentration, moment, and anisotropy. Nano Res 9(9):2772–2781

Geng BQ, Ma YQ, Xu YF, Xu ST, Sun X, Zheng GH, Dai ZX (2015) Separated $CoFe_2O_4$/CoFe nanoparticles by the SiOx matrix: revealing the intrinsic origin for the small remanence magnetization. J Nanopart Res 17:281

Geng BQ, Ma YQ, Xu ST, Xu YF, Sun X, Dai ZX, Zheng GH (2016b) High magnetic performance of cobalt ferrite and anomalous magnetizing behavior of $CoFe_2$/oxide derived from ferrite. Ceram Int 42:317–324

Hamid Z, Ahmad Khalid F (2011) Exchange coupling and magnetic behavior of SmCo5 − xSnx alloys. J Mater Sci Technol 27:218–222

Ji JY, Shih PH, Chan TS, Ma YR, Wu SY (2015) Magnetic properties of cluster glassy Ni/NiO core–shell nanoparticles: an investigation of their static and dynamic magnetization. Nanoscale Res Lett 10:243

Kooti M, Naghdi Sedeh A (2013) Synthesis and characterization of $NiFe_2O_4$ magnetic nanoparticles by combustion method. J Mater Sci Technol 29:34–38

Li WM, Wong SK, Herng TS, Yap LK, Sim CH, Yang ZC, Chen YJ, Shi JZ, Han GC, Xue JM (2015) Perpendicular magnetic clusters with configurable domain structures via dipole–dipole interactions. Nano Res 8:3639–3650

Liu YH, Velthuis SGET, Jiang JS, Choi Y, Bader SD, Parizzi AA, Ambaye H, Lauter V (2011) Magnetic structure in Fe/Sm-Co exchange spring bilayers with intermixed interfaces. Phys Rev B 83:174418

López-Ortega A, Estrader M, Salazar-Alvarez G, Roca AG, Nogués J (2015) Applications of exchange coupled bimagnetic hard/soft and soft/hard magnetic core/shell nanoparticles. Plasma Phys Rep 553:1–32

Mousavand T, Naka T, Sato K, Ohara S, Umetsu M, Takami S, Nakane T, Matsushita A, Adschiri T (2009) Crystal size and magnetic field effects in Co_3O_4 antiferromagnetic nanocrystals. Phys Rev B 79:144411

Mathieu HM, Nordblad P, Binns C, Baker S (2013) Memory effects on the magnetic behavior of assemblies of nanoparticles with ferromagnetic core/antiferromagnetic shell morphology. Phys Rev B 88:140402

Nadeem K, Krenn H, Sarwar W, Mumtaz M (2014) Comparison of surface effects in SiO_2 coated and uncoated nickel ferrite nanoparticles. Appl Surf Sci 288:677–681

Ou-Yang J, Zhang Y, Luo XN, Yan BQ, Zhu BP, Yang XF, Chen S (2015) Composition dependence of the magnetic properties of $CoFe_2O_4/CoFe_2$ composite nano-ceramics. Ceram Int 41: 3896–3900

Petracic O, Chen X, Bedanta S, Kleemann W, Sahoo S, Cardoso S, Freitas PP (2006) Collective states of interacting ferromagnetic nanoparticles. J Magn Magn Mater 300:192–197

Pianciola Betiana N, Jr EL, Troiani Horacio E, Nagamine Luiz CCM, Cohen R, Zysler Roberto D (2015) Size and surface effects in the magnetic order of $CoFe_2O_4$ nanoparticles. J Magn Magn Mater 377:44–51

Qin RH, Li FS, Jiang W, Liu L (2009) Salt-assisted low temperature solid state synthesis of high surface area $CoFe_2O_4$ nanoparticles. J Mater Sci Technol 25:69–72

Quesada A, Rubio-Marcos F, Marco JF, Mompean FJ, García-Hernández M, Fernández JF (2014) On the origin of remanence enhancement in exchange-uncoupled CoFe2O4-based composites. Appl Phys Lett 105:202405

Ramis Mustafa Ö, Umut S, Mustafa Y, Hakan Ç (2014) Characterization of microstructural and morphological properties in As-deposited Ta/NiFe/IrMn/CoFe/Ta multilayer system. J Mater Sci Technol 30:359–364

Soares JM, Cabral FAO, Araújo JH d, Machado FLA (2011) Exchange-spring behavior in nanopowders of $CoFe_2O_4$–$CoFe_2$. Appl Phys Lett 98:072502

Soares JM, Galdino VB, Machado FLA (2014) Exchange-bias and exchange-spring coupling in magnetic core–shell nanoparticles. J Magn Magn Mater 350:69–72

Sun X, Ma YQ, Xu YF, Xu ST, Geng BQ, Dai ZX, Zheng GH (2015) Improved magnetic performance at low and high temperatures in non-exchange-coupling $CoFe_2O_4/CoFe_2$ nanocomposites. J Alloys Compd 645:51–56

Verma S, Pravarthana D (2011) One-pot synthesis of highly monodispersed ferrite nanocrystals: surface characterization and magnetic properties. Langmuir 27:13189–13197

Wang SJ, Zhao X, Xiao N, Zuo L (2012) High magnetic field influence on the Widmanst¨atten transformation in high purity Fe–0.36 wt% C alloy. J Mater Sci Technol 28:552–557

Xia AL, Ren SZ, Lin JS, Ma Y, Xu C, Li JL, Jin CG, Liu XG (2015) Magnetic properties of sintered $SrFe_{12}O_{19}$-$CoFe_2O_4$ nanocomposites with exchange coupling. J Alloys Compd 653:108–116

Xu ST, Ma YQ, Xu YF, Sun X, Geng BQ, Zheng GH, Dai ZX (2015a) Pure dipolar-interacted $CoFe_2O_4$ nanoparticles and their magnetic properties. Mater Res Bull 62:142–147

Xu YF, Ma YQ, Xu ST, Zheng GH, Dai ZX (2015b) Diluted and undiluted monodispersed $CoFe_2O_4$ nanoparticles: the effects of post-annealing on magnetic properties. J Mater Sci 50: 4486–4494

Xu ST, Ma YQ, Zheng GH, Dai ZX (2015c) Simultaneous effects of surface spins: rarely large coercivity, high remanence magnetization and jumps in the hysteresis loops observed in $CoFe_2O_4$ nanoparticles. Nanoscale 7:6520–6526

Zhang Y, Lin J, Wen DJ (2011) Structure, infrared radiation properties and Mössbauer spectroscopic investigations of $Co_{0.6}Zn_{0.4}NixFe_2 - xO_4$ ceramics. J Mater Sci Technol 26: 687–692

Zan FL, Ma YQ, Ma Q, Zheng GH, Dai ZX, Wu MZ, Li G, Sun ZQ, Chen XS (2013a) One-step hydrothermal synthesis and characterization of high magnetization $CoFe_2O_4/Co_{0.7}Fe_{0.3}$ nanocomposite permanent magnets. J Alloy Compd 553: 79–85

Zan FL, Ma YQ, Ma Q, Xu YF, Dai ZX, Zheng GH, Wu MZ, Li G (2013b) Magnetic and impedance properties of nanocomposite $CoFe_2O_4/Co_{0.7}Fe_{0.3}$ and single phase $CoFe_2O_4$ via one-step hydrothermal. J Am Ceram Soc 96:3100–3107

Zhang Y, Yang Z, Zhu BP, Chen S, Yang XF, Xiong R, Liu Y (2013) Exchange-spring effect in $CoFe_2O_4/CoFe_2$ composite nano-particles. J Alloys Compd 567:73–76

Zehani K, Bez R, Boutahar A, Hlil EK, Lassri H, Moscovici J, Mliki N, Bessais L (2014) Structural, magnetic, and electronic properties of high moment FeCo nanoparticles. J Alloys Compd 591:58–64